NANO LETTERS

pubs.acs.org/NanoLett
Letter

Electrically Switching Ferroelectric Order in 3R-MoS_2 Layers

Tianyi Ouyang, Soonyoung Cha, Yiyang Sun, Takashi Taniguchi, Kenji Watanabe, Nathaniel M. Gabor,* and Chun Hung Lui*

Cite This: *Nano Lett.* 2025, 25, 1459−1465

ABSTRACT: Transition metal dichalcogenides (TMDs) with rhombohedral (3R) stacking order are excellent platforms to realize multiferroelectricity. In this work, we demonstrate the electrical switching of ferroelectric orders in bilayer, trilayer, and tetralayer 3R-MoS_2 dual-gate devices by examining their reflection and photoluminescence (PL) responses under sweeping out-of-plane electric fields. We observe sharp shifts in excitonic spectra at different critical fields with pronounced hysteresis. These phenomena are attributed to distinct interlayer polarizations resulting from specific lateral displacements between the layers, with each configuration yielding a unique ferroelectric state. Our findings indicate two, three, and four ferroelectric regimes for bilayer, trilayer, and tetralayer structures, respectively, in agreement with theoretical prediction. Moreover, each polarization state can be stabilized at zero applied electric field. The tunable ferroelectric phases of these multilayers pave the way for innovative applications in non-volatile memory, logic circuits, and optoelectronic devices.

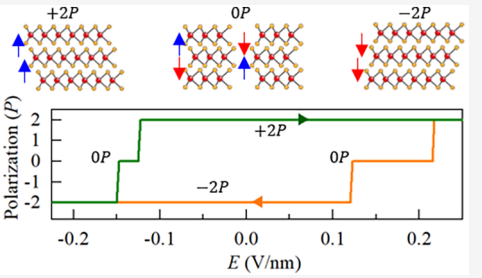

KEYWORDS: *transition metal dichalcogenides, MoS_2, 3R stacking, ferroelectric order, multiferroelectricity, electrical switching*

The stacking sequence of layers is critical in defining the properties of two-dimensional (2D) materials. While most studies focus on the common Bernal or 2H stacking with 180° interlayer twisting, the less common rhombohedral (3R) sequence offers unique material properties and novel phenomena.[1−5] For instance, rhombohedral multilayer graphene can exhibit flat bands, strongly correlated states and superconductivity.[6−8] For transition metal dichalcogenides (TMDs) like MoS_2 and WSe_2, 3R-stacked multilayers provide an excellent platform for realizing multiferroelectricity. In 3R-MoS_2 layers, for instance, the Mo atoms in one layer align vertically with the S atoms in the adjacent layer (Figure 1b-c). The difference in electronic affinity between Mo and S leads to charge transfer, resulting in a permanent out-of-plane electric dipole. Interestingly, sliding the layers by one intralayer Mo−S bond-length (0.242 nm) reverses the interlayer Mo−S alignment, creating an opposite electric dipole, thus allowing the realization of two opposite ferroelectric orders in bilayer 3R-MoS_2.[9,10] As the layer thickness increases, the number of ferroelectric states grows significantly due to the numerous ways to displace the layers, presenting an exciting opportunity for multiferroelectricity in 2D materials.[11−13] Such ferroelectricity has been demonstrated in 3R layers, both artificially stacked[14−18] and coherently stacked crystals, showing photovoltaic effects,[19−21] enhanced nonlinear optical response[22−25] and electric-field-driven switching behavior.[26−28] However, the impact of multiferroelectricity on optical responses remains underexplored and warrants detailed investigation.

In this paper, we demonstrate electrical switching of ferroelectric orders in bilayer, trilayer, and tetralayer 3R-MoS_2 by measuring their reflection and photoluminescence (PL) response under a sweeping out-of-plane electric field. We observe abrupt changes in the excitonic spectra at discrete critical fields, indicating phase transitions. Reversing the electric field direction reveals pronounced hysteresis, a hallmark of ferroelectric behavior. These phenomena are attributed to distinct interlayer polarizations induced by specific translational displacements between 3R-stacked MoS_2 layers. Our results reveal two, three, and four ferroelectric regimes in bilayer, trilayer, and tetralayer 3R-MoS_2, respectively, consistent with the anticipated number of distinct interlayer polarizations in these structures. Notably, by manipulating the sweeping fields, we can stabilize each ferroelectric polarization state at zero applied electric field. The electrically controllable multiferroelectricity holds promise for novel device applications, including next-generation non-volatile memory and optoelectronic sensors. Compared to recent studies focusing on the reflection response of trilayer 3R-MoS_2,[11,29] our work encompasses bi-, tri-, and tetra-layer 3R-MoS_2, integrates reflection and PL responses, and demonstrates the stabilization of intermediate ferroelectric

Received: October 28, 2024
Revised: December 17, 2024
Accepted: January 2, 2025
Published: January 14, 2025

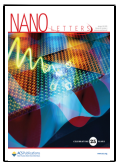

https://doi.org/10.1021/acs.nanolett.4c05370
Nano Lett. 2025, 25, 1459−1465

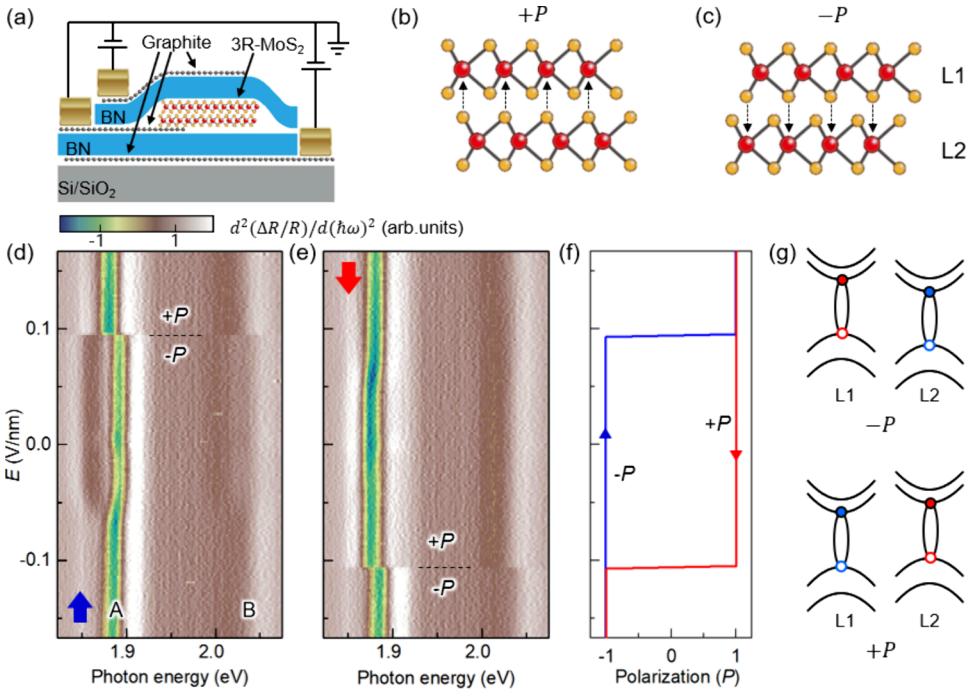

Figure 1. Switching ferroelectric order in bilayer 3R-MoS_2. (a) The schematic of dual-gate 3R-MoS_2 device (b-c) Bilayer stacking configurations with polarizations $\pm P$. (d-e) Color map of the second-order energy derivative of reflectance contrast spectra of bilayer 3R-MoS_2 device under opposite electric-field sweeping directions (denoted by the red and blue arrows). Distinct ferroelectric regimes with opposite interlayer polarizations $\pm P$ are denoted. The dashed lines denote the critical fields at which the ferroelectric order switches. The A and B excitons are denoted. (f) The bilayer ferroelectric hysteresis extracted from Panels d-e. (g) Schematic K-valley band structures of individual layers (L1 and L2) in bilayer 3R-MoS_2. A potential difference between the two layers is induced by the interlayer polarization of the ferroelectric order.

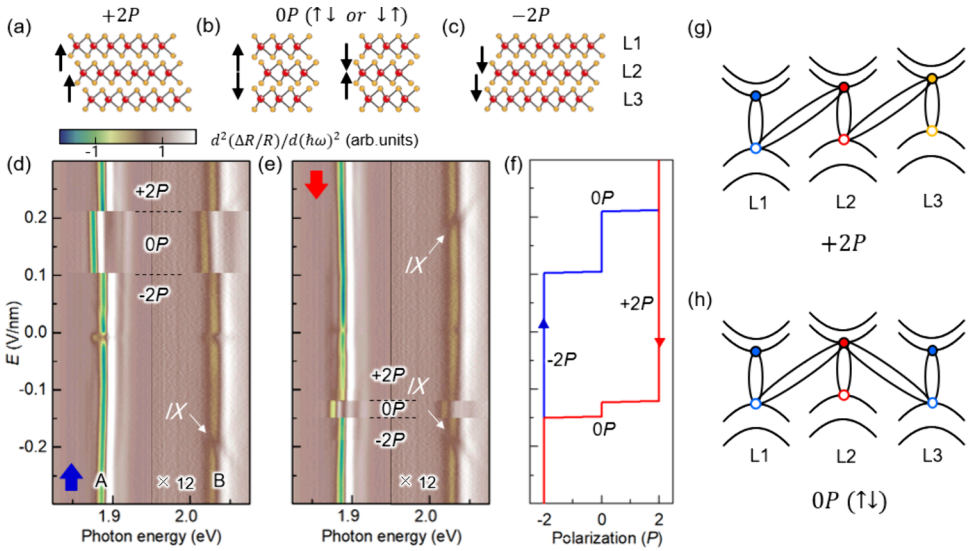

Figure 2. Switching ferroelectric order in trilayer 3R-MoS_2. (a-c) Trilayer stacking configurations with $0P$, $\pm 2P$ polarizations. (d-e) Color maps of the second-order energy derivative of reflectance contrast spectra of trilayer 3R-MoS_2 device under opposite electric-field sweeping directions (denoted by the red and blue arrows). Distinct ferroelectric regimes with interlayer polarizations $0P$, $\pm 2P$ are denoted. The dashed lines denote the critical fields at which the ferroelectric order switches. As the B exciton feature near 2.03 eV is quite weak, we have enhanced it by magnifying the value above 1.95 eV for 12 times in both maps. (f) The trilayer ferroelectric hysteresis extracted from Panels d-e. (g-h) Schematic K-valley band structure of individual layers (L1, L2, L3) in trilayer 3R-MoS_2 at $+2P$ and $0P$ polarizations.

states. These advancements provide new insights and broaden the scope of ferroelectric phenomena in 2D materials.

We fabricate 3R-MoS_2 dual-gate devices encapsulated with hexagonal boron nitride (BN) on Si/SiO_2 substrates (Figure 1a). Thin graphite flakes serve as contacts and electrodes to enhance device performance. By applying gate voltages of opposite signs on the top and bottom gates, vertical electric fields are applied to the MoS_2 samples with minimal or no charge injection. Reflectance contrast ($\Delta R/R$) and PL measurements are conducted under varying electric fields at a sample temperature of $T = 6$ K. Additionally, we calculate the second-order energy derivative $d^2(\Delta R/R)/d(\hbar\omega)^2$ of the

https://doi.org/10.1021/acs.nanolett.4c05370
Nano Lett. 2025, 25, 1459−1465

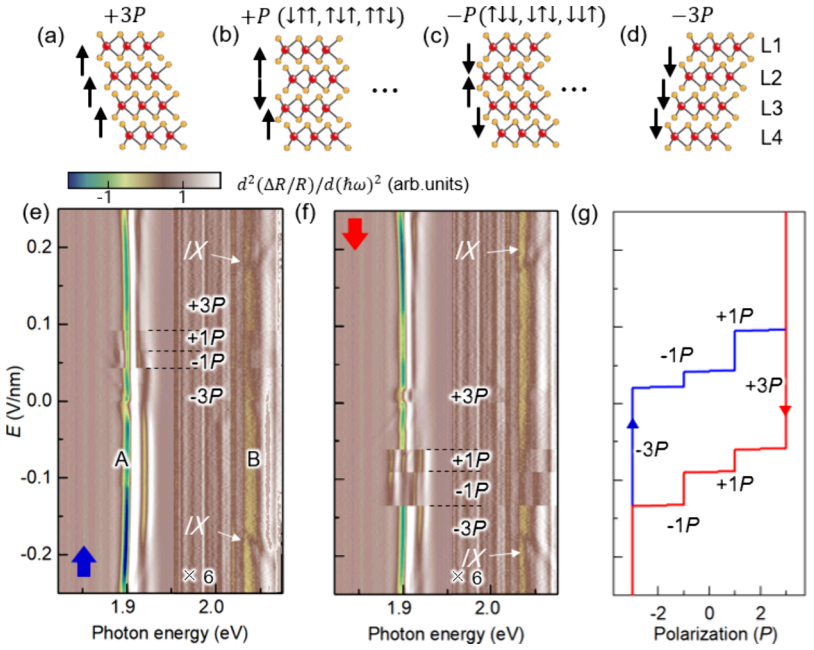

Figure 3. Switching ferroelectric order in tetralayer 3R-MoS_2. (a-d) Tetralayer stacking configurations with $\pm P$, $\pm 3P$ polarizations. (e-f) Color maps of the second-order energy derivative of reflectance contrast spectra of tetralayer 3R-MoS_2 under opposite electric-field sweeping directions (denoted by the red and blue arrows). Distinct ferroelectric regimes with interlayer polarizations $\pm P$, $\pm 3P$ are denoted. The dashed lines denote the critical fields at which the ferroelectric order switches. As the B exciton feature near 2.03 eV is quite weak, we have enhanced it by magnifying the value above 1.96 eV for 6 times in both maps. (g) The tetralayer ferroelectric hysteresis extracted from Panels e-f.

reflection contrast spectra to enhance weak spectral features. Detailed device fabrication and experimental procedures are provided in the Supporting Information. The following sections present the results for bilayer, trilayer, and tetralayer 3R-MoS_2 devices in sequence.

First, we examine the properties and results of the bilayer. In a 3R-MoS_2 bilayer, when the Mo atoms in Layer One (L1) align with the S atoms in Layer Two (L2), charge transfer between them induces a spontaneous dipole moment (P) pointing from L2 to L1 (Figure 1b). However, if L1 is laterally displaced by one intralayer Mo−S bond length, the S atoms in L1 will align with the Mo atoms in L2, creating an opposite dipole moment ($-P$) (Figure 1c). In a pristine bilayer, the $\pm P$ ferroelectric phases are related by mirror symmetry and theoretically should exhibit identical excitonic spectra. However, realistic bilayer devices often have layer-imbalanced charges that break this symmetry, resulting in slight excitonic spectral differences between the $\pm P$ phases.

This subtle difference is observed in the $d^2(\Delta R/R)/d(\hbar\omega)^2$ maps of our bilayer Device 01. In Figure 1d, when the electric field (E) is swept from negative to positive, an abrupt change occurs at E = 0.095 V/nm in the spectral lines of A exciton (1.88 eV) and B exciton (2.02 eV), indicating a phase transition. Conversely, when sweeping the field from positive to negative, similar changes are noted at E = −0.106 V/nm. The results show pronounced hysteresis, as depicted in Figure 1f. These sharp spectral changes and hysteresis match the expected behavior of ferroelectric switching in bilayer 3R-MoS_2.[9,26]

The ferroelectric order becomes richer in trilayer 3R-MoS_2, which can exhibit three distinct interlayer polarizations with $+2P$, $0P$, and $-2P$ dipole moment (Figure 2a-c). For the $+2P$ polarization (Figure 2a), the three layers are displaced sequentially, aligning the Mo atoms in L1 (L2) with the S atoms in L2 (L3). This creates a $+P$ polarization between L1 and L2 and between L2 and L3, resulting in a total $+2P$ polarization for the trilayer. For the $0P$ polarization (Figure 2b), the three layers are displaced in a zigzag pattern, aligning Mo atoms in L1 and L3 with S atoms in L2 (or S atoms in L1 and L3 with Mo atoms in L2). This creates opposite polarizations between L1 and L2 and between L2 and L3, resulting in zero net polarization. Finally, for the $-2P$ polarization (Figure 2c), the S atoms in L1 (L2) align with the Mo atoms in L2 (L3), creating a $-P$ polarization for each interface.

The $d^2(\Delta R/R)/d(\hbar\omega)^2$ maps for trilayer 3R-MoS_2 Device 02 reveal three distinct regimes, separated by abrupt spectral changes at two critical electric fields. In Figure 2d, sweeping the electric field from negative to positive causes changes of the A and B exciton lines at E = 0.10 and 0.21 V/nm, indicating two phase transition. Similar changes occur when the field is swept in the reverse direction (Figure 2e). The results show pronounced hysteresis (Figure 2f), consistent with ferroelectric switching in trilayer 3R-MoS_2. For comparison, we also measured bilayer and trilayer MoS_2 with 2H stacking order but observed no abrupt spectral shifts under a sweeping electric field (Figure S9, Supporting Information). This contrast underscores the critical role of the 3R stacking order in enabling the ferroelectric switching phenomenon.

The ferroelectric order in tetralayer 3R-MoS_2 becomes increasingly complex, exhibiting four distinct interlayer polarizations $+3P$, $+P$, $-P$, and $-3P$ (Figure 2a-c). For the $+3P$ polarization (Figure 3a), the four layers are displaced so that the Mo atoms in L1, L2, L3 align with the S atoms in L2, L3, L4, respectively. This arrangement generates three $+P$ interfacial polarizations, resulting in a total dipole moment of $+3P$ for the tetralayer. The $+P$ polarization (Figure 3b) can be achieved through three different stacking configurations, where the four layers are displaced in a zigzag pattern, creating alternative interfacial polarizations, such as ($-P$,$+P$,$+P$), ($+P$,$-$

https://doi.org/10.1021/acs.nanolett.4c05370
Nano Lett. 2025, 25, 1459−1465

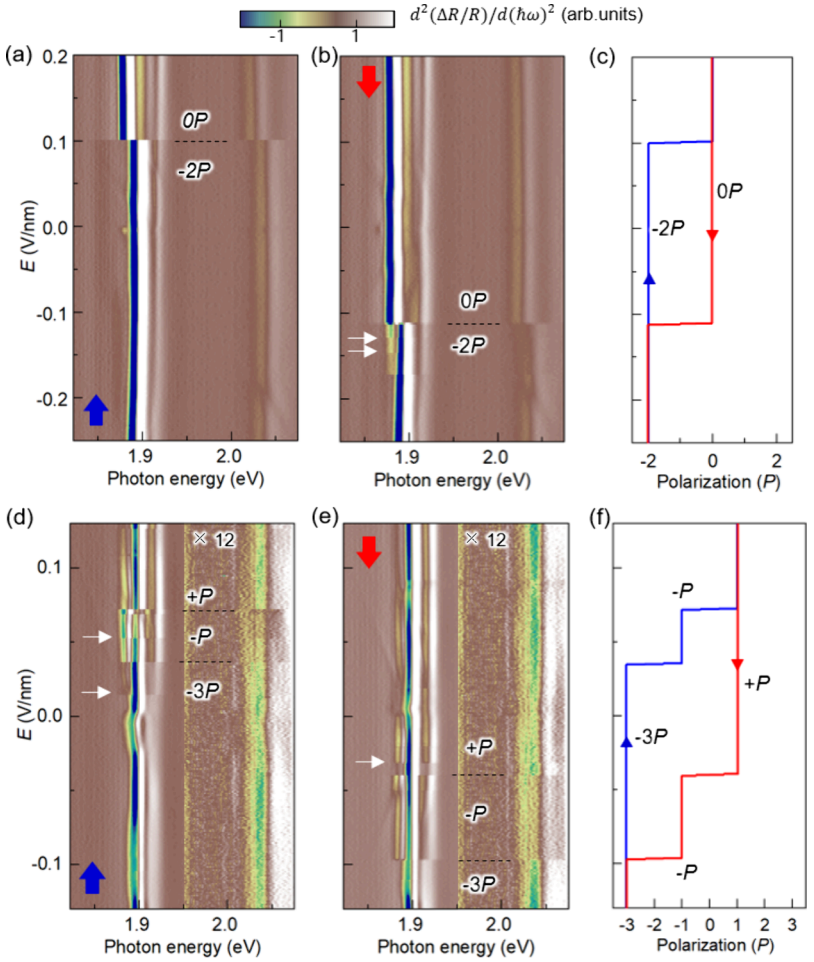

Figure 4. Stabilizing intermediate ferroelectric orders at zero applied electric field. (a-b) Color maps of the second-order energy derivative of reflectance contrast spectra of trilayer 3R-MoS_2 under opposite electric-field sweeping directions (denoted by the red and blue arrows). (c) Ferroelectric hysteresis extracted from Panels a-b. (d-f) Similar maps and hysteresis for tetralayer 3R-MoS_2 Device. As the B exciton feature near 2.03 eV is quite weak, we have enhanced it by magnifying the value above 1.95 eV for 12 times in both maps. The white arrows in Panels b, d, e highlight possible domain effects.

P,+P) and (+P,+P,−P). Similarly, the −P and −3P polarizations are obtained by reversing the +P and +3P configurations (Figure 3c-d). The $d^2(\Delta R/R)/d(\hbar\omega)^2$ maps for our tetralayer 3R-MoS_2 Device 03 show four distinct regimes, marked by abrupt spectral changes at three critical electric fields (Figure 3e-f). The results also display pronounced hysteresis when the electric field is swept in the opposite direction (Figure 3g), consistent with the expected ferroelectric switching behavior in tetralayer 3R-MoS_2.

Following the identification of distinct ferroelectric polarizations, we demonstrate how to stabilize each polarization state at zero applied electric field. In the trilayer case, the 0P intermediate state is typically observed only at finite electric field in Figure 2. However, we find partial hysteresis between the 0P and −2P (or +2P) states (Figure 4a-c). After reaching the 0P state, if the electric field is swept reversely, the 0P state can be maintained even at zero applied electric field. A similar partial hysteresis exists between different ferroelectric phases in the tetralayer, enabling the stabilization of each intermediate state at zero field (Figure 4d-f).

We observe some minor abrupt spectral changes in our maps while sweeping the electric field, highlighted by the white arrows in Figure 4b, d, and e. These features suggest the presence of multiple ferroelectric domains within the sample. As the electric field increases, certain domains undergo polarization flipping earlier, causing subtle shifts in optical signals, while others flip at higher fields, resulting in more pronounced changes. Further investigation with spatially resolved probes is warranted to elucidate the characteristics of the ferroelectric domains in 3R-MoS_2.

Previous discussions have focused on reflection contrast results related to the absorption properties of intralayer excitons. Ferroelectric orders also significantly influence emission properties, as shown in the PL maps of trilayer and tetralayer 3R-MoS_2 (Figure 5). Unlike absorption properties that are dominated by the intralayer excitons at the K valley, the emission properties are governed by intervalley excitons at lower energies.[30,31] In the trilayer, strong PL is observed near 1.3 eV, attributed to indirect excitons between the K and Γ valleys,[9,32,33] which can recombine with the assistance of defects or phonons.[34] We observe abrupt changes in PL spectra at two distinct electric fields, accompanied by pronounced hysteresis (Figure 5a-c). The PL results are consistent to the existence of three distinct ferroelectric polarizations in trilayer. In the tetralayer, the PL spectra become more complex as the Q valley drops slightly below the K valley in the conduction band,[32,35] leading to the emission of QΓ excitons in addition to the KΓ excitons. These QΓ and KΓ

https://doi.org/10.1021/acs.nanolett.4c05370
Nano Lett. 2025, 25, 1459−1465

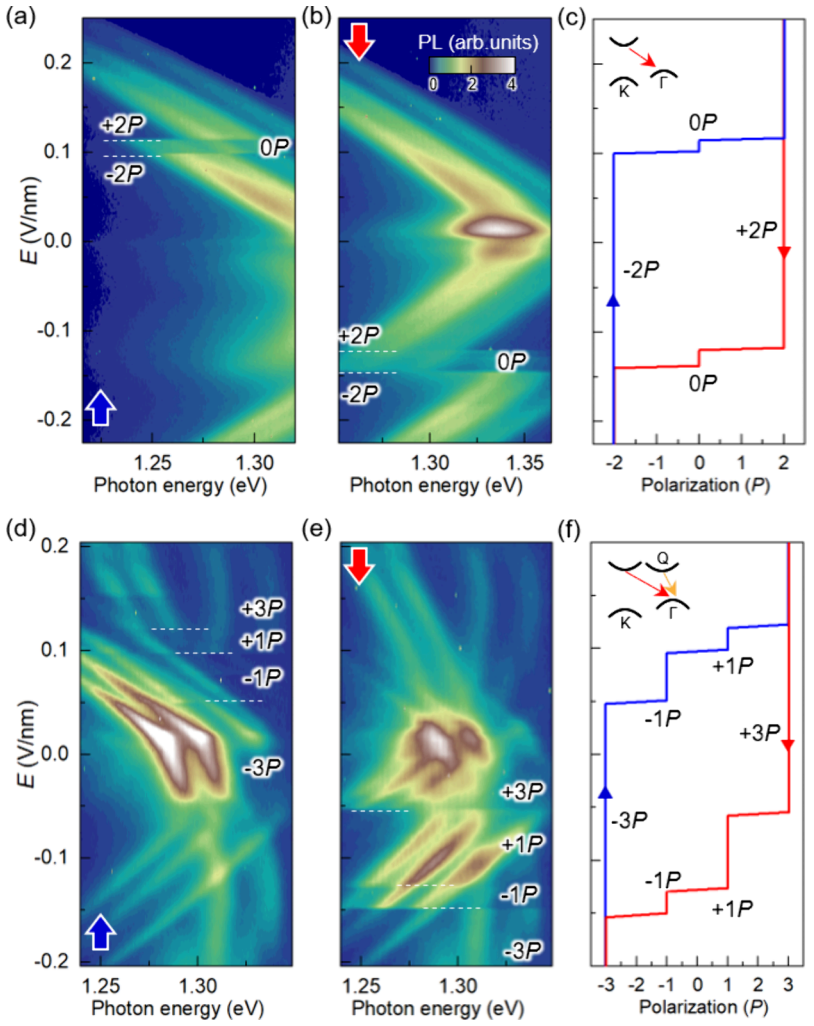

Figure 5. Photoluminescence (PL) signatures of ferroelectric switching in trilayer and tetralayer 3R-MoS_2. (a-b) PL maps of the trilayer 3R-MoS_2 device under opposite electric-field sweeping directions (denoted by the red and blue arrows). Distinct ferroelectric regimes with interlayer polarizations 0*P*, ±2*P* are denoted. The dashed lines denote the critical fields at which the ferroelectric order switches. (c) The trilayer ferroelectric hysteresis extracted from Panels a-b. The inset shows a schematic band configuration of KΓ exciton responsible for the trilayer PL. (d-f) Similar maps and hysteresis for the tetralayer 3R-MoS_2 device. The inset in Panel f shows a schematic band configuration of KΓ and QΓ excitons responsible for the tetralayer PL. All PL spectra in Panels a, b, d, e share the same color scale in Panel b.

excitons can be distinguished by their distinct Stark shift. We observe abrupt PL spectral changes at three critical electric fields with hysteresis (Figure 5d-f), consistent with the presence of four distinct ferroelectric polarizations in the tetralayer. Both the trilayer and tetralayer PL results demonstrate that ferroelectric switching significantly impacts the emission properties of excitons in 3R-MoS_2.

In addition to ferroelectric switching, we observe pronounced K-valley interlayer excitons (IX) in the reflectance contrast maps of trilayer and tetralayer (Figures 2, 3). These excitons exhibit Stark shifts with an extracted dipole of approximately 0.6 *e·nm*, which is close to the expected dipole of a bilayer interlayer exciton given the interlayer spacing of ~0.6 nm in MoS_2. These interlayer excitons are typically dark due to electron−hole separation (Figure 2g-h). Moreover, group theory analysis indicates that, in bilayer, trilayer and tetralayer 3R-MoS_2, all interlayer excitons between adjacent layers are forbidden from coupling with the intralayer A and B excitons because they belong to different irreducible representations under 3-fold rotational symmetry. However, our results show that the K-valley interlayer excitons become bright when they align energetically with the B excitons. This anomalous brightening suggests that the coupling between intra- and interlayer excitons is mediated by symmetry-breaking defects (see the Supporting Information for more discussion).

In summary, we demonstrate the electrical switching of ferroelectric orders in bilayer, trilayer, and tetralayer 3R-MoS_2 through reflection and photoluminescence (PL) measurements under varying out-of-plane electric fields. Abrupt excitonic spectral changes at critical fields signal phase transitions, while hysteresis upon reversing the field confirms ferroelectric behavior. These phenomena arise from distinct interlayer polarizations caused by translational displacements between layers, with each stacking configuration producing a unique ferroelectric phase. Our study identifies two, three, and four ferroelectric regimes for bilayer, trilayer, and tetralayer structures, consistent with theoretical predictions, and suggests even more complex orders in thicker 3R-MoS_2 samples. Furthermore, we demonstrate that each ferroelectric polarization can be stabilized at zero applied field. The tunable ferroelectric properties of 3R-MoS_2 multilayers open new

https://doi.org/10.1021/acs.nanolett.4c05370
Nano Lett. 2025, 25, 1459−1465

avenues for applications in non-volatile memory, logic circuits, and optoelectronic devices. The ability to control multiple polarization states and excitonic coupling, particularly through symmetry-breaking defects, offers significant potential for developing advanced photodetectors and sensors.

■ ASSOCIATED CONTENT

Supporting Information

The Supporting Information is available free of charge at https://pubs.acs.org/doi/10.1021/acs.nanolett.4c05370.

Details on the device fabrication, reflection contrast and photoluminescence measurements, calculation of the interlayer electric field, discussion on stacking configurations of tetralayer 3R-MoS_2, and symmetry analysis on multilayer 3R-MoS_2 based on group theory (PDF)

■ AUTHOR INFORMATION

Corresponding Authors

Nathaniel M. Gabor − *Department of Physics and Astronomy, University of California Riverside, Riverside, California 92521, United States;* orcid.org/0000-0002-0351-2787; Email: nathaniel.gabor@ucr.edu

Chun Hung Lui − *Department of Physics and Astronomy, University of California Riverside, Riverside, California 92521, United States*; Email: joshua.lui@ucr.edu

Authors

Tianyi Ouyang − *Department of Physics and Astronomy, University of California Riverside, Riverside, California 92521, United States;* orcid.org/0009-0005-5928-4778

Soonyoung Cha − *Department of Physics and Astronomy, University of California Riverside, Riverside, California 92521, United States;* orcid.org/0009-0009-9973-0372

Yiyang Sun − *Department of Physics and Astronomy, University of California Riverside, Riverside, California 92521, United States*

Takashi Taniguchi − *Research Center for Materials Nanoarchitectonics, National Institute for Materials Science, Tsukuba 305-0044, Japan;* orcid.org/0000-0002-1467-3105

Kenji Watanabe − *Research Center for Electronic and Optical Materials, National Institute for Materials Science, Tsukuba 305-0044, Japan;* orcid.org/0000-0003-3701-8119

Complete contact information is available at: https://pubs.acs.org/10.1021/acs.nanolett.4c05370

Author Contributions

T.O. and S.C. contributed equally to this work.

Notes

The authors declare no competing financial interest.

■ ACKNOWLEDGMENTS

C.H.L. acknowledges support from the National Science Foundation (NSF) Division of Materials Research CAREER Award No. 1945660. K.W. and T.T. acknowledge support from the JSPS KAKENHI (Grant Numbers 21H05233 and 23H02052) , the CREST (JPMJCR24A5), JST and World Premier International Research Center Initiative (WPI), MEXT, Japan. N.M.G. and S.C. were supported by ARO MURI grant No. W911NF-24-1-0292 and the Army Research Office Electronics Division Award No. W911NF-21-1-0260. N.M.G. was also supported by the Presidential Early Career Award for Scientists and Engineers (PECASE) through the Air Force Office of Scientific Research (award No. FA9550-20-1-0097).

■ REFERENCES

(1) Li, L.; Wu, M. Binary compound bilayer and multilayer with vertical polarizations: two-dimensional ferroelectrics, multiferroics, and nanogenerators. *ACS Nano* **2017**, *11*, 6382−6388.

(2) Ji, J.; Yu, G.; Xu, C.; Xiang, H. J. General theory for bilayer stacking ferroelectricity. *Phys. Rev. Lett.* **2023**, *130*, No. 146801.

(3) Bennett, D.; Remez, B. On Electrically Tunable stacking domains and ferroelectricity in moiré superlattices. *npj 2D Mater. Appl.* **2022**, *6*, 7.

(4) Bennett, D. Theory of polar domains in moiré heterostructures. *Phys. Rev. B* **2022**, *105*, No. 235445.

(5) Wu, M.; Li, J. Sliding ferroelectricity in 2D van der Waals materials: related physics and future opportunities. *Proc. Natl. Acad. Sci. U. S. A.* **2021**, *118*, No. e2115703118.

(6) Zhou, H.; Xie, T.; Taniguchi, T.; Watanabe, K.; Young, A. F. Superconductivity in rhombohedral trilayer graphene. *Nature* **2021**, *598*, 434−438.

(7) Han, T.; Lu, Z.; Scuri, G.; Sung, J.; Wang, J.; Han, T.; Watanabe, K.; Taniguchi, T.; Fu, L.; Park, H.; Ju, L. Orbital multiferroicity in pentalayer rhombohedral graphene. *Nature* **2023**, *623*, 41−47.

(8) Vinas Bostrom, E.; Fischer, A.; Profe, J. B.; Zhang, J.; Kennes, D. M.; Rubio, A. Phonon-mediated unconventional superconductivity in rhombohedral stacked multilayer graphene. *npj Comput. Mater.* **2024**, *10*, 163.

(9) Liang, J.; Yang, D.; Wu, J.; Dadap, J. I.; Watanabe, K.; Taniguchi, T.; Ye, Z. Optically probing the asymmetric interlayer coupling in rhombohedral-stacked MoS_2 bilayer. *Phys. Rev. X* **2022**, *12*, No. 041005.

(10) Sung, J.; Zhou, Y.; Scuri, G.; Zólyomi, V.; Andersen, T. I.; Yoo, H.; Wild, D. S.; Joe, A. Y.; Gelly, R. J.; Heo, H.; et al. Broken mirror symmetry in excitonic response of reconstructed domains in twisted $MoSe_2$/$MoSe_2$ bilayers. *Nat. Nanotechnol.* **2020**, *15*, 750−754.

(11) Deb, S.; Krause, J.; Faria Junior, P. E.; Kempf, M. A.; Schwartz, R.; Watanabe, K.; Taniguchi, T.; Fabian, J.; Korn, T. Excitonic signatures of ferroelectric order in parallel-stacked MoS_2. *Nat. Commun.* **2024**, *15*, 7595.

(12) Deb, S.; Cao, W.; Raab, N.; Watanabe, K.; Taniguchi, T.; Goldstein, M.; Kronik, L.; Urbakh, M.; Hod, O.; Ben Shalom, M. Cumulative polarization in conductive interfacial ferroelectrics. *Nature* **2022**, *612*, 465−469.

(13) Cao, W.; Deb, S.; Stern, M. V.; Raab, N.; Urbakh, M.; Hod, O.; Kronik, L.; Shalom, M. B. Polarization saturation in multilayered interfacial ferroelectrics. *Adv. Mater.* **2024**, *36*, No. 2400750.

(14) Molino, L.; Aggarwal, L.; Enaldiev, V.; Plumadore, R.; Fal'ko, I.; Luican-Mayer, A. Ferroelectric switching at symmetry-broken interfaces by local control of dislocations networks. *Adv. Mater.* **2023**, *35*, No. 2207816.

(15) Ko, K.; Yuk, A.; Engelke, R.; Carr, S.; Kim, J.; Park, D.; Heo, H.; Kim, H.-M.; Kim, S.-G.; Kim, H.; et al. Operando electron microscopy investigation of polar domain dynamics in twisted van der Waals homobilayers. *Nat. Mater.* **2023**, *22*, 992−998.

(16) Woods, C. R.; Ares, P.; Nevison-Andrews, H.; Holwill, M. J.; Fabregas, R.; Guinea, F.; Geim, A. K.; Novoselov, K. S.; Walet, N. R.; Fumagalli, L. Charge-polarized interfacial superlattices in marginally twisted hexagonal boron nitride. *Nat. Commun.* **2021**, *12*, 347.

(17) Wang, X.; Yasuda, K.; Zhang, Y.; Liu, S.; Watanabe, K.; Taniguchi, T.; Hone, J.; Fu, L.; Jarillo-Herrero, P. Interfacial ferroelectricity in rhombohedral-stacked bilayer transition metal dichalcogenides. *Nat. Nanotechnol.* **2022**, *17*, 367.

(18) Weston, A.; Castanon, E. G.; Enaldiev, V.; Ferreira, F.; Bhattacharjee, S.; Xu, S.; Corte-Leon, H.; Wu, Z.; Clark, N.; et al. Interfacial ferroelectricity in marginally twisted 2D semiconductors. *Nat. Nanotechnol.* **2022**, *17*, 390−395.

(19) Yang, D.; Wu, J.; Zhou, B. T.; Liang, J.; Ideue, T.; Siu, T.; Awan, K. M.; Watanabe, K.; Taniguchi, T.; Iwasa, Y.; Franz, M.; Ye, Z. Spontaneous-polarization-induced photovoltaic effect in rhombohedrally stacked MoS_2. *Nat. Photonics* **2022**, *16*, 469−474.
(20) Wu, J.; Yang, D.; Liang, J.; Werner, M.; Ostroumov, E.; Xiao, Y.; Watanabe, K.; Taniguchi, T.; Dadap, J. I.; Jones, D.; Ye, Z. Ultrafast response of spontaneous photovoltaic effect in 3R-MoS_2-based heterostructures. *Sci. Adv.* **2022**, *8*, No. eade3759.
(21) Dong, Y.; Yang, M.-M.; Yoshii, M.; Matsuoka, S.; Kitamura, S.; Hasegawa, T.; Ogawa, N.; Morimoto, T.; Ideue, T.; Iwasa, Y. Giant bulk piezophotovoltaic effect in 3R-MoS_2. *Nat. Nanotechnol.* **2023**, *18*, 36−41.
(22) Zeng, Z. X. S.; Sun, X. X.; Zhang, D. L.; Zheng, W. H.; Fan, X. P.; He, M.; Xu, T.; Sun, L. T.; Wang, X.; Pan, A. L. Controlled vapor growth and nonlinear optical applications of large-area 3R phase WS_2 and WSe_2 atomic layers. *Adv. Funct. Mater.* **2019**, *29*, No. 1806874.
(23) Wang, L.; Qi, J.; Wei, W.; Wu, M.; Zhang, Z.; Li, X.; Sun, H.; Guo, Q.; Cao, M.; Wang, Q.; et al. Bevel-edge epitaxy of ferroelectric rhombohedral boron nitride single crystal. *Nature* **2024**, *629*, 74−79.
(24) Hsu, W.-T.; Zhao, Z.-A.; Li, L.-J.; Chen, C.-H.; Chiu, M.-H.; Chang, P.-S.; Chou, Y.-C.; Chang, W.-H. Second harmonic generation from artificially stacked transition metal dichalcogenide twisted bilayers. *ACS Nano* **2014**, *8*, 2951−2958.
(25) Rogee, L.; Wang, L.; Zhang, Y.; Cai, S.; Wang, P.; Chhowalla, M.; Ji, W.; Lau, S. P. Ferroelectricity in untwisted heterobilayers of transition metal dichalcogenides. *Science* **2022**, *376*, 973.
(26) Yang, D.; Liang, J.; Wu, J.; Xiao, Y.; Dadap, J. I.; Watanabe, K.; Taniguchi, T.; Ye, Z. Non-volatile electrical polarization switching via domain wall release in 3R-MoS_2 bilayer. *Nat. Commun.* **2024**, *15*, 1389.
(27) Meng, P.; Wu, Y.; Bian, R.; Pan, E.; Dong, B.; Zhao, X.; Chen, J.; Wu, L.; Sun, Y.; Fu, Q.; et al. Sliding induced multiple polarization states in two-dimensional ferroelectrics. *Nat. Commun.* **2022**, *13*, 7696.
(28) Liang, J.; Yang, D.; Xiao, Y.; Chen, S.; Dadap, J. I.; Rottler, J.; Ye, Z. Shear strain-induced two-dimensional slip avalanches in rhombohedral MoS_2. *Nano Lett.* **2023**, *23*, 7228−7235.
(29) Liang, J.; Yang, D.; Wu, J.; Xiao, Y.; Watanabe, K.; Taniguchi, T.; Dadap, J. I.; Ye, Z. Resolving polarization switching pathways of sliding ferroelectricity in trilayer 3R-MoS_2. *arXiv* 2024, *2410*, 02973.
(30) Mak, K. F.; Lee, C.; Hone, J.; Shan, J.; Heinz, T. F. Atomically thin MoS_2: A new direct-gap semiconductor. *Phys. Rev. Lett.* **2010**, *105*, No. 136805.
(31) Splendiani, A.; Sun, L.; Zhang, Y.; Li, T.; Kim, J.; Chim, C. Y.; Galli, G.; Wang, F. Emerging photoluminescence in monolayer MoS_2. *Nano Lett.* **2010**, *10*, 1271−1275.
(32) Kormányos, A.; Zólyomi, V.; Fal'ko, V. I.; Burkard, G. Tunable Berry curvature and valley and spin Hall effect in bilayer MoS_2. *Phys. Rev. B* **2018**, *98*, No. 035408.
(33) Li, Z.; Förste, J.; Watanabe, K.; Taniguchi, T.; Urbaszek, B.; Baimuratov, A. S.; Gerber, I. C.; Högele, A.; Bilgin, I. Stacking-dependent exciton multiplicity in WSe_2 bilayers. *Phys. Rev. B* **2022**, *106*, No. 045411.
(34) Altaiary, M. M.; Liu, E.; Liang, C.-T.; Hsiao, F.-C.; van Baren, J.; Taniguchi, T.; Watanabe, K.; Gabor, N. M.; Chang, Y.-C.; Lui, C. H. Electrically switchable intervalley excitons with strong two-phonon scattering in bilayer WSe_2. *Nano Lett.* **2022**, *22* (5), 1829−1835.
(35) Akashi, R.; Ochi, M.; Bordács, S.; Suzuki, R.; Tokura, Y.; Iwasa, Y.; Arita, R. Two-dimensional valley electrons and excitons in noncentrosymmetric 3R-MoS_2. *Phys. Rev. Applied* **2015**, *4*, No. 014002.

https://doi.org/10.1021/acs.nanolett.4c05370
Nano Lett. 2025, 25, 1459−1465